Modelling HTS coils with different coupling scenarios via integral method

Calvin C. T. Chow, Min Zhang, K. T. Chau, and Francesco Grilli

***Abstract*—High-temperature superconducting (HTS) tapes can be stacked together to form cables which are then wound into coils for potential use in electrical machines. The tapes in the cable can either be uncoupled (insulated from each other), coupled-at-ends (coupled at the terminals of the cable), or fully coupled (electrically connected with each other). The integral method can readily model the uncoupled scenario, and this paper extends the integral method to model the coupled-at-ends and fully coupled scenarios. We find that the proposed method has a time advantage over the well-established T-A formulation of Maxwell's equations.**

***Index Terms*—HTS modelling, integral method, J-model, multi-tape superconducting cable**

I. Introduction

High-temperature superconducting (HTS) tapes can be used in the armature of electrical machines [1]–[7]. To wind coils in the armature of electrical machines, HTS tapes can be stacked to form a cable which is then wound into coils. The tapes in the cable can be insulated from each other or electrically connected with each other, and there is insulation between cable turns. As in the literature [8], [9], we analyze three different coupling scenarios of a coil wound from a cable:

1) Uncoupled: the tapes in the cable are insulated from each other, and there is a separate power supply for each tape at the terminals. Each tape turn in the coil carries the same transport current.
2) Coupled-at-ends: tapes are insulated from each other in the cable, but tapes of the cable are soldered together at the terminals of the cable.
3) Coupled: tapes in the cable are electrically connected along the whole length of the cable.

In all three scenarios above, there is insulation between adjacent cable turns.

The decision to use which of the above winding method depends on various factors. Using a multi-tape cable to wind a coil can give high current-carrying capacity [2], [10] and decrease the inductance of the coil [8]. A high current rating is needed for high-power electrical machines, and cannot be substituted by having more turns and increasing the voltage in cases where voltage has to be limited, e.g., in electric aircraft due to safety reasons. Pardo *et al.* [8] showed that for the armature of an electrical machine, among the three coupling scenarios, the uncoupled case had the lowest ac loss, followed by the coupled-at-ends case and followed by the coupled case. Taking note of the advantages of non-insulated coils [11], [12], a coupled coil may have the advantage of thermal stability and reduced susceptibility to quenching because current around local hotspots can be diverted to other tapes in the same cable turn.

This paper addresses the problem of numerically modelling the loss in the HTS layers in the coupled-at-ends and coupled scenarios; the uncoupled scenarios can readily be modelled since the current in each tape turn is known and is given by the injected current. From the literature, the H-formulation (in which magnetic field strength $\mathbf{H}$ is the variable being solved for) can model the coupled-at-ends and coupled scenarios easily by current constraints [9]. Zermano *et al.* [13] used the H-formulation for the coupled-at-ends scenario. The Minimum Electro-Magnetic Entropy Production (MEMEP) method has also been used for the three coupling scenarios [8]. In terms of the T-A formulation (in which current vector potential $\mathbf{T}$ and magnetic vector potential $\mathbf{A}$ are the variables being solved for), Wang *et al.* [14] developed a new way of using Neumann boundary conditions on each tape and an integral constraint for the total current of the cable to model a cable when current in each tape is not known before computation and thus cannot be specified in the Dirichlet boundary conditions. On the other hand, Santos *et al.* [9] coupled the conventional T-A formulation with an equivalent circuit so the current in each tape calculated from the circuit is fed back into the T formulation.

The integral method was proposed by Brandt [15] and involved solving the current density in each meshed element in the superconducting domain, based on an integral equation that involves the current density. The integral method is faster than the T-A formulation [16], [17]. However, like the conventional T-A formulation, the conventional integral method requires the current in each tape turn to be known. In this paper, we extend the integral method to the two coupled scenarios where the current in each tape is not known before computation. We do this by extracting the necessary constraints (on the current and voltage of the tape turns) from the equivalent circuit representations of the tapes given by Santos *et al.* [9].

This work was supported in part by two grants (Project Numbers 17204021 and T23-701/20-R) from the Hong Kong Research Grants Council, Hong Kong Special Administrative Region, China. *(Corresponding author: min.zhang@strath.ac.uk)*

Calvin C. T. Chow was a visitor at the Department of Electronics and Electrical Engineering, University of Strathclyde, G1 1XQ Glasgow, United Kingdom, and is with the Department of Electrical and Electronic Engineering, The University of Hong Kong, Pokfulam, Hong Kong SAR, China. Min Zhang is with the Department of Electronics and Electrical Engineering, University of Strathclyde, G1 1XQ Glasgow, United Kingdom. K. T. Chau is with the Research Centre for Electric Vehicles and Department of Electrical and Electronic Engineering, The Hong Kong Polytechnic University, Hung Hom, Kowloon, Hong Kong SAR, China. Francesco Grilli is with the Institute for Technical Physics (ITEP), Karlsruhe Institute of Technology (KIT), 76131 Karlsruhe, Germany.

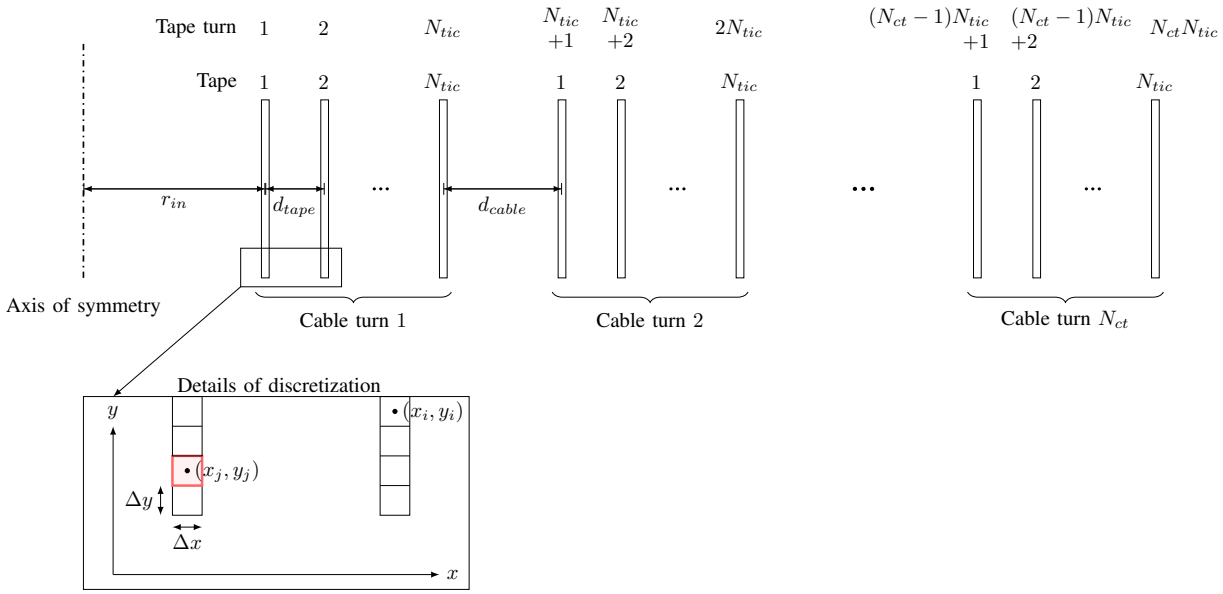

Fig. 1: Arrangement of tapes in one side of a coil with N_{ct} cable turns, made of a cable consisting of N_{tic} tapes stacked together.

The rest of the paper is organized as follows. Section II specifies the situation being modelled and introduces key equations from the integral method that are needed for this paper. Section III explains how we extend the integral method to the coupled scenarios by specifying appropriate constraints. Section IV shows simulations results for a coil under the different coupling scenarios. Section V suggests, as future work, how contact resistance can be modelled and how the equivalent circuit used in this paper can be coupled with a numerical method other than the integral method. We conclude in Section VI.

II. Problem Set-up and Introduction to the Integral Method

A. Geometry modelled

This paper considers a 2D model of the straight section(s) of a racetrack coil made up of winding a cable N_{ct} turns (thus N_{ct} cable turns), and the cable consists of N_{tic} tapes stacked together, as shown in Fig. 1. There are $N_t = N_{ct}N_{tic}$ tape turns in total. The tapes can be uncoupled, coupled-at-ends, or coupled as in the introduction. The cable carries a transport current $I_{set}(t)$; in the uncoupled case, each tape carries a current $I_{set}(t)/N_{tic}$.

Only the superconducting layer of each tape turn is modelled in this paper. Let the superconducting domain modelled be S, which consists of the superconducting layer of every tape turn. Each tape turn area is discretized into a single layer of rectangular elements, and every element has same size Δx and Δy along the x and y axes, respectively, as shown in Fig. 1. Within each element, the electromagnetic quantities, such as the magnetic vector potential $\mathbf{A}$, current density $\mathbf{J}$, and electric field strength $\mathbf{E}$, are constant. Therefore, we assume that electromagnetic quantities do not vary across the width of a tape; however, the 2D nature of the elements is considered when doing area integration in equations in Section II-B. Let N_e be the number of elements that the superconducting domain S is discretized into. Let the centre of the element i be $\mathbf{r}_i = (x_i, y_i), i = 1, ..., N_e$.

Due to the 2D geometry adopted,

$$\mathbf{A}, \mathbf{J}, \mathbf{E} = \{A(x, y, t), J(x, y, t), E(x, y, t)\}\hat{\mathbf{z}} \tag{1}$$

At any one point, let $A = A_J + A_a$, where A_J is the magnetic vector potential due to current in superconductor domain S, and A_a is the magnetic vector potential due to external magnetic field created by sources other than current in S.

From $\mathbf{B} = \nabla \times \mathbf{A}$, where $\mathbf{B}$ is the magnetic flux density, and Faraday's law $\nabla \times \mathbf{E} = -\frac{\partial \mathbf{B}}{\partial t}$, we see that $\nabla \times (\mathbf{E} + \frac{\partial \mathbf{A}}{\partial t}) = 0$ so $\mathbf{E} + \frac{\partial \mathbf{A}}{\partial t}$ is a conservative field and can be described by the gradient of a scalar potential: $-\nabla\phi = \mathbf{E} + \dot{\mathbf{A}}$. Under our 2D geometry, $E + \dot{A} = -\frac{\partial \phi}{\partial z}$. The potential difference per unit tape length into page, $\frac{\partial \phi}{\partial z}$, in our 2D model can be supplied by an external voltage source when the tape is connected to a power supply.

B. Key equations from integral method

The integral method was originally developed by Brandt [15] and is a method to solve for the evolution of current density in superconductors. In this subsection, we summarize key equations as reviewed in [17], starting with[1]

$$\begin{aligned}\dot{J}(\mathbf{r}) = &-\frac{1}{\mu_0}\int_S Q^{-1}(\mathbf{r}, \mathbf{r}')\left[E(\mathbf{r}') + \dot{A}_a(\mathbf{r}')\right] d^2r' \\ &-\frac{1}{\mu_0}\sum_{j=1}^{N_t}\frac{\partial \phi(\Omega_j)}{\partial z}\int_{\Omega_j} Q^{-1}(\mathbf{r}, \mathbf{r}')\, d^2r',\end{aligned} \tag{2}$$

[1]Note that $\nabla^2 \dot{A}_a$ in (14) of [17] is zero as explained in the same article.

where $Q(\mathbf{r},\mathbf{r}') = -\frac{1}{2\pi}\ln|\mathbf{r}-\mathbf{r}'|$ is the Green function for 2D; $Q^{-1}(\mathbf{r},\mathbf{r}')$ is defined by $\int_S Q^{-1}(\mathbf{r},\mathbf{r}')Q(\mathbf{r}',\mathbf{r}'')\,d^2r' = \delta(\mathbf{r}-\mathbf{r}'')$; $\frac{\partial\phi(\Omega_j)}{\partial z}$ is uniform in space in each tape turn area $\Omega_j, j = 1,2,...,N_t$, due to reasons explained in [18]. For more compact notation, for the rest of this paper,

$$\left(\frac{\partial\phi}{\partial z}\right)_j := \frac{\partial\phi(\Omega_j)}{\partial z} = \frac{\partial\phi(\mathbf{r})}{\partial z}\ \forall\mathbf{r}\in\Omega_j. \tag{3}$$

The electric field $E(\mathbf{r})$ is related to $J(\mathbf{r})$ by $E-J$ power law

$$E = E_c\left|\frac{J}{J_c}\right|^n\frac{J}{|J|}, \tag{4}$$

where J_c is the critical current density of the HTS layer, E_c is taken to be 10^{-4} V m^{-1}, and n determines how steep the $E-J$ relation is.

In the discretized geometry, (2) is evaluated at the centre of each discretized element, i.e., at $\mathbf{r}=\mathbf{r}_i, i=1,2,...,N_e$, so we get N_e equations, which can be collected into matrix form [17]

$$\underline{\dot{J}} = \underline{\underline{Q_{inv}}}(\underline{E}+\underline{\dot{A}_a}) + \underline{\underline{Q_{inv}}}\,\underline{\underline{L}}^T\frac{\partial\underline{\phi}}{\partial z}, \tag{5}$$

where $\underline{\underline{Q_{inv}}} = -\frac{1}{\mu_0\Delta x\Delta y}\underline{\underline{Q}}^{-1}$ with $\underline{\underline{Q}}$ defined as $\left[\underline{\underline{Q}}\right]_{ij} = \int_{\Omega_j}Q(\mathbf{r}_i,\mathbf{r}')\,d^2r'\frac{1}{\Delta x\Delta y}$; $\underline{\underline{L}}$ is an $N_t\times N_e$ matrix whose element $\left[\underline{\underline{L}}\right]_{ij}=1$, if the element j belongs to turn i and $=0$ otherwise. $\underline{\dot{J}}$, $\underline{E}$, and $\underline{\dot{A}_a}$ are $N_e\times 1$ vectors whose elements are $[\underline{\dot{J}}]_i = \dot{J}(\mathbf{r}_i)$, $[\underline{E}]_i = E(\mathbf{r}_i)$, $\left[\underline{\dot{A}_a}\right]_i = \dot{A}_a(\mathbf{r}_i)$, respectively. $\frac{\partial\underline{\phi}}{\partial z}$ is a $N_t\times 1$ vector with $\left[\frac{\partial\underline{\phi}}{\partial z}\right]_i = \left(\frac{\partial\phi}{\partial z}\right)_i$.

Equation (5) can be solved, for example by the forward Euler method used in the Python code for Section IV, to find the time evolution of J in all the elements, provided we give an expression for $\frac{\partial\underline{\phi}}{\partial z}$. The expression $\frac{\partial\underline{\phi}}{\partial z}$ contains the elements $\left[\frac{\partial\underline{\phi}}{\partial z}\right]_i = \left(\frac{\partial\phi}{\partial z}\right)_i$ and so there are in total N_t unknowns, i.e., $\left(\frac{\partial\phi}{\partial z}\right)_i, i=1,2,...,N_t$.

The focus of Section III is to find an expression for $\frac{\partial\underline{\phi}}{\partial z}$ for the coupled-at-ends and coupled scenarios, and below we include the expression for $\frac{\partial\underline{\phi}}{\partial z}$ for the uncoupled case as derived in [16] and reviewed in [17].

When tapes are uncoupled, the current in each tape turn is known, which is equal to the externally applied current, and thus we can impose the N_t current constraints [16]: for $i=1,2,...,N_t$,

$$\frac{\dot{I}_{set}(t)}{N_{tic}} = \int_{\Omega_i}\dot{J}(\mathbf{r},t)\,d^2r. \tag{6}$$

Let us define I_i to be the current in tape turn $i=1,2,...,N_t$, and substituting (2),

$$\begin{aligned}\dot{I}_i &:= \int_{\Omega_i}\dot{J}(\mathbf{r},t)\,d^2r\\ &= \int_{\Omega_i}s(\mathbf{r},t)\,d^2r\\ &\quad -\sum_{j=1}^{N_t}\left[\left(\frac{\partial\phi(t)}{\partial z}\right)_j\frac{1}{\mu_0}\int_{\Omega_i}\int_{\Omega_j}Q^{-1}(\mathbf{r},\mathbf{r}')\,d^2r'\,d^2r\right],\end{aligned} \tag{7}$$

where $s(\mathbf{r},t) = -\frac{1}{\mu_0}\int_S Q^{-1}(\mathbf{r},\mathbf{r}')[E(\mathbf{r}')+\dot{A}_a(\mathbf{r}')]\,d^2r'$.

Substitute (7) into (6), we get [16], [17]: for $i=1,2,...,N_t$,

$$\begin{aligned}&-\sum_{j=1}^{N_t}\left[\left(\frac{\partial\phi(t)}{\partial z}\right)_j\frac{1}{\mu_0}\int_{\Omega_i}\int_{\Omega_j}Q^{-1}(\mathbf{r},\mathbf{r}')\,d^2r'\,d^2r\right]\\ &= \frac{\dot{I}_{set}(t)}{N_{tic}} - \int_{\Omega_i}s(\mathbf{r},t)\,d^2r.\end{aligned} \tag{8}$$

Applying discretization and collecting the N_t equations of (8), one for each tape turn $i=1,2,...,N_t$, we can find the N_t unknowns by solving [16], [17]:

$$\underline{\underline{M_u}}\frac{\partial\underline{\phi}}{\partial z} = \underline{P_u} \tag{9}$$

$$\frac{\partial\underline{\phi}}{\partial z} = \underline{\underline{M_u}}^{-1}\underline{P_u}, \tag{10}$$

where $\underline{\underline{M_u}} = \Delta x\Delta y\underline{\underline{L}}\,\underline{\underline{Q_{inv}}}\,\underline{\underline{L}}^T$, $\underline{P_u} = \frac{\dot{I}_{set}(t)}{N_{tic}}\underline{1} - \underline{\underline{L}}\,\underline{\underline{Q_{inv}}}(\underline{E}+\underline{\dot{A}_a})\Delta x\Delta y$ and $\underline{1}$ is a vector of 1's. The subscript u stands for "uncoupled".

III. Applying Appropriate Constraints in Coupled Scenarios

In this section, we explain how to find the N_t unknowns $\left(\frac{\partial\phi}{\partial z}\right)_i, i=1,2,...,N_t$, for the coupled-at-ends and the coupled scenarios. Under the coupled-at-ends and coupled scenarios, we cannot readily impose the N_t current constraints (6), since the current in each tape turn area is not known before computation.

Santos *et al.* [9] examined the relationships between the current, I_i and voltage per meter, $\left(\frac{\partial\phi}{\partial z}\right)_i$ of each tape turn for the coupled-at-ends and coupled scenarios and presented the relationships in the form of circuit diagrams. In Santos *et al.* [9], the cross-sectional area of each tape turn i is represented as a circuit element (which we call R_i in this paper) with current I_i through it, and with the voltage across it being the mean of $E+\dot{A}$ multiplied by 1 m evaluated at the discretized elements of the tape turn[2]. The current-voltage relationship for R_i is provided by the coupling between the circuit model and the T-A formulation[3] [9].

[2]Note $E+\dot{A} = \left(\frac{\partial\phi}{\partial z}\right)_i$, which is the unknown we want, and in this paper we will interpret the voltage across the circuit element R_i as voltage per meter $\left(\frac{\partial\phi}{\partial z}\right)_i$.

[3]Current calculated from the electrical circuit is imposed as the constraint in the T formulation (implemented in the partial differential equation module in COMSOL); voltage, which is the average $E+\dot{A}$ (times an arbitrary length of 1 m) of the elements of a tape turn, is extracted from the A formulation (implemented via the magnetic field module in COMSOL) and fed into the electrical circuit.

A main contribution of this paper is to extract from these circuit diagrams [9] the necessary constraints on I_i and $\left(\frac{\partial \phi}{\partial z}\right)_i$ and formulate the constraints mathematically into the form of (9). Thus, the N_t unknowns $\left(\frac{\partial \phi}{\partial z}\right)_i$ can be determined in the integral method for the coupled-at-ends and coupled scenarios.

A. Coupled-at-ends

As explained by Santos *et al.* [9], in the coupled-at-ends case, tape turns that are part of the same physical tape have the same current through them, and thus those tape turns are connected in series in the equivalent circuit. The equivalent circuit for a coil with N_{ct} cable turns of a cable consisting of N_{tic} coupled-at-ends tapes is given in Fig. 2.

From Fig. 2, we extract the following three sets of conditions needed to find the N_t unknowns $\left(\frac{\partial \phi}{\partial z}\right)_i$ for the integral method.

1) The sum of current of all tape turns in the first cable turn (or any other cable turns) is equal to the applied current on the cable. In the circuit in Fig. 2, this corresponds to the fact that sum of currents through $R_i, i = 1, 2, ..., N_{tic}$ sum to I_{set}. Thus,
$$\sum_{i=1}^{N_{tic}} \dot{I}_i = \dot{I}_{set}. \tag{11}$$
This gives us one equation.
2) Tape turns that are part of the same physical tape have the same current through them. In the circuit in Fig. 2, this corresponds to the fact that all R_i belonging to the same tape are in series. Thus, for each tape $i = 1, 2, ..., N_{tic}$ in a cable,
$$\dot{I}_i = \dot{I}_{i+N_{tic}} = \dot{I}_{i+2N_{tic}} = ... = \dot{I}_{i+(N_{ct}-1)N_{tic}} \tag{12}$$
There are $N_{ct} - 1$ equations in (12), and (12) applies to each of N_{tic} tapes, thus this second set of constraints gives us in total $(N_{ct} - 1)N_{tic}$ equations.
3) The sum of the voltages across all tape turns that belong to a tape is the same for all tapes in the cable, since the tapes in the cable are coupled at the ends of the cable. In the circuit in Fig. 2, this corresponds to the fact that the branches that represent tapes (each branch containing the R_i of the tape in different cable turns) are in parallel with each other, thus sharing the same voltage. Thus,
$$\sum_{j=0}^{N_{ct}-1} \left(\frac{\partial \phi}{\partial z}\right)_{1+jN_{tic}} = \sum_{j=0}^{N_{ct}-1} \left(\frac{\partial \phi}{\partial z}\right)_{2+jN_{tic}} = ... = \sum_{j=0}^{N_{ct}-1} \left(\frac{\partial \phi}{\partial z}\right)_{N_{tic}+jN_{tic}}. \tag{13}$$
This third set of constraints gives us in total $N_{tic} - 1$ equations.

Note the first and second sets of equations can be written in terms of $\left(\frac{\partial \phi}{\partial z}\right)_i$ since $\dot{I}_i$ can be written in terms of $\left(\frac{\partial \phi}{\partial z}\right)_i$ according to (7). Therefore, there are in total $1 + (N_{ct} - 1)N_{tic} + N_{tic} - 1 = N_{ct}N_{tic} = N_t$ equations, allowing us to solve for the N_t unknowns. These N_t equations can be collected into matrix form, like (9), as
$$\underline{\underline{M_{cae}}}\,\underline{\frac{\partial \phi}{\partial z}} = \underline{P_{cae}}, \tag{14}$$
where subscripts cae stand for "coupled-at-ends". Thus, we can solve for the N_t unknowns in $\underline{\frac{\partial \phi}{\partial z}}$. Details of entries in $\underline{\underline{M_{cae}}}$ and $\underline{P_{cae}}$ are given in Appendix A.

B. Coupled

As explained by Santos *et al.* [9], in the coupled case, each tape turn in a cable is in electrical contact and thus tape turns in a cable turn are connected in parallel in the equivalent circuit. The equivalent circuit for a coil with N_{ct} cable turns of a cable consisting of N_{tic} coupled tapes is given in Fig. 2 (considering the dashed lines as solid lines in the figure). We have assumed that there is zero contact resistance between the tapes in a cable turn, as reflected by the fact that the tapes in a cable turn are connected in parallel with no resistor on the dashed lines.

From Fig. 2, we extract the following two sets of conditions needed to find the N_t unknowns $\left(\frac{\partial \phi}{\partial z}\right)_i$ for the integral method.

1) The voltages across all tape turns within a cable turn are the same. This is reflected by the fact that all R_i belonging to the same cable turn are in parallel. Thus, for each cable turn $i = 1, 2, ..., N_{ct}$,
$$\left(\frac{\partial \phi}{\partial z}\right)_{m+1} = \left(\frac{\partial \phi}{\partial z}\right)_{m+2} = ... = \left(\frac{\partial \phi}{\partial z}\right)_{m+N_{tic}}, \quad m = (i-1)N_{tic}. \tag{15}$$
There are $N_{tic} - 1$ equations in (15), and (15) applies to N_{ct} cable turns, so this first set of constraints gives us $(N_{tic} - 1)N_{ct}$ equations.
2) The sum of current through all tape turns in a cable turn is equal to the current applied to the cable. This is reflected in the circuit diagram as we can see that $I_{set} = \sum_{l=1}^{N_{tic}} I_{(k-1)N_{tic}+l}$ for each cable turn $k = 1, 2, ..., N_{ct}$. Thus, taking time derivatives, for each cable turn $k = 1, 2, ..., N_{ct}$
$$\dot{I}_{set} = \sum_{l=1}^{N_{tic}} \dot{I}_{(k-1)N_{tic}+l}. \tag{16}$$
Equation (16) applies to each of the N_{ct} cable turns, so this second set of constraints gives us N_{ct} equations.

The second set of equations can be written in terms of $\left(\frac{\partial \phi}{\partial z}\right)_i$ since $\dot{I}_i$ can be written in terms of $\left(\frac{\partial \phi}{\partial z}\right)_i$ according to (7). Therefore, there are in total $(N_{tic} - 1)N_{ct} + N_{ct} = N_{tic}N_{ct} = N_t$ equations, allowing us to solve for the N_t unknowns. These N_t equations can be collected into matrix form, like (9), as
$$\underline{\underline{M_c}}\,\underline{\frac{\partial \phi}{\partial z}} = \underline{P_c}, \tag{17}$$
where subscript c stands for "coupled". Thus, we can solve for the N_t unknowns in $\underline{\frac{\partial \phi}{\partial z}}$. Details of entries in $\underline{\underline{M_c}}$ and $\underline{P_c}$ are given in Appendix B.

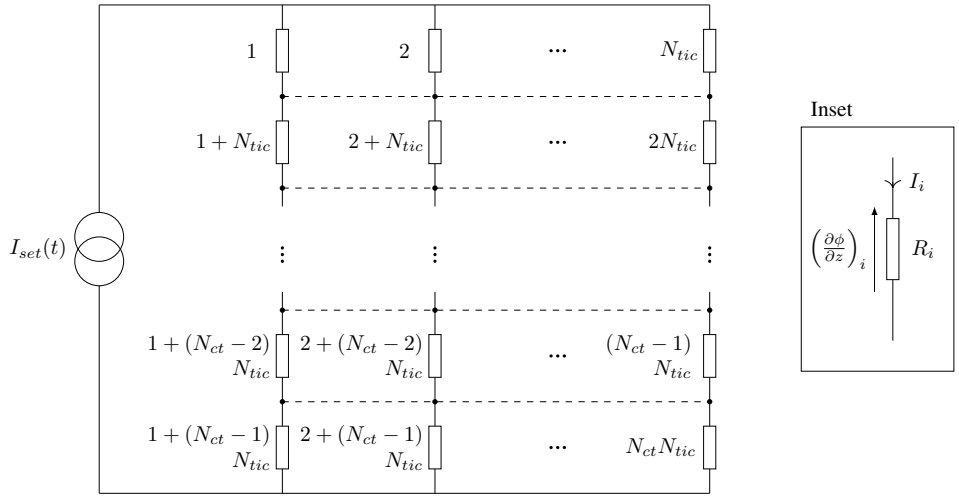

Fig. 2: Equivalent circuit representing the relationship between current and voltage of each tape turn for the coupled-at-ends (ignoring the dashed lines) and coupled (including the dashed lines) scenarios based on [9]. The label next to each resistor is the tape turn number. The inset shows the meaning of the variables used in this paper.

IV. Validation

In this section, we compare the ac loss of a racetrack coil carrying transport ac under the three coupling scenarios. The coil has $N_{ct} = 4$ cable turns and the cable is made of $N_{tic} = 16$ tapes. The transport current carried by the cable is set to be $I_{set} = I_0 \sin(2\pi ft)$, where $f = 500$ Hz. The tape parameters and geometry are the same as in Santos *et al.* [9], with a constant critical current density J_c. Details of the coil parameters are given in Table I. In the following simulations, only one straight section of the coil is built in the geometry of the 2D models, and the other side of the coil is taken into account by symmetry. The ac loss values are for one side of the coil only.

First, we simulate the three coupling scenarios for two periods (0.004 s) with $I_0 = 0.8I_c$, where I_c is the critical current of a tape multiplied by number of tapes in the cable. We use three different methods and compare their results: the integral method presented in this paper, the T-A formulation and the H-formulation. The integral method is implemented in Python; the T-A formulation is implemented in COMSOL using the method described in Santos *et al.* [9]; and the H-formulation is implemented in COMSOL, using "Global Constraints" to specify current of tapes in each coupling scenario. The current distribution at the instant $t = 0.001$ s calculated by the integral method and the T-A formulation is plotted in Fig. 3, and they agree with each other. Further, the instantaneous ac loss of each scenario, and the time taken by each method, are presented in Fig. 4. Each curve from the integral method consists of 2001 data points joined together, and each curve from the T-A formulation and the H-formulation consists of 201 data points joined together. The oscillations of curves of the integral method do not affect average ac loss, as shown in Fig. 5. The T-A formulation and the H-formulation have been validated with each other [9], and here we can see the integral method agrees with them as well. Since the time taken by the H-formulation is longer than the T-A formulation, we only compare the integral method with the T-A formulation below.

TABLE I: Simulation parameters

Description	Unit	Value
Tape properties		
Tape width	mm	4
Tape thickness	μm	2
Critical current density	Am^{-2}	2.1959×10^{10}
Critical current	A	175.67
n	-	30
No. of elements per tape (Python, Matlab, COMSOL)	-	80
Coil properties (refer to Fig. 1)		
Number of tapes in cable, N_{tic}	-	16
Number of cable turns, N_{ct}	-	4
Distance between adjacent tapes (centre-to-centre) in a cable turn, d_{tape}	mm	2.413/15
Distance from tape at end of a cable turn to tape at start of next cable turn, d_{cable}	mm	0.358
Inner radius of coil, r_{in}	mm	15

Second, we vary amplitude I_0 from 20% to 100% of I_c and simulate the ac loss for 1 period (0.02 s). The average ac loss results in the second half of the period simulated are plotted in Fig. 5, and excellent agreement can be seen between the integral method and the T-A formulation. The time taken by both methods are given in Fig. 6, and the integral method takes 45% or less of the time taken by the T-A formulation in all cases.

V. Possible extension and future work

A. Modelling contact resistance and termination resistance

The termination resistance of electrical contact at the ends of the coil are modelled in Zermeno *et al.* [13] as a resistance in an equivalent circuit, or a per unit resistance term contribution to the E field in the H formulation. Adapting such approaches

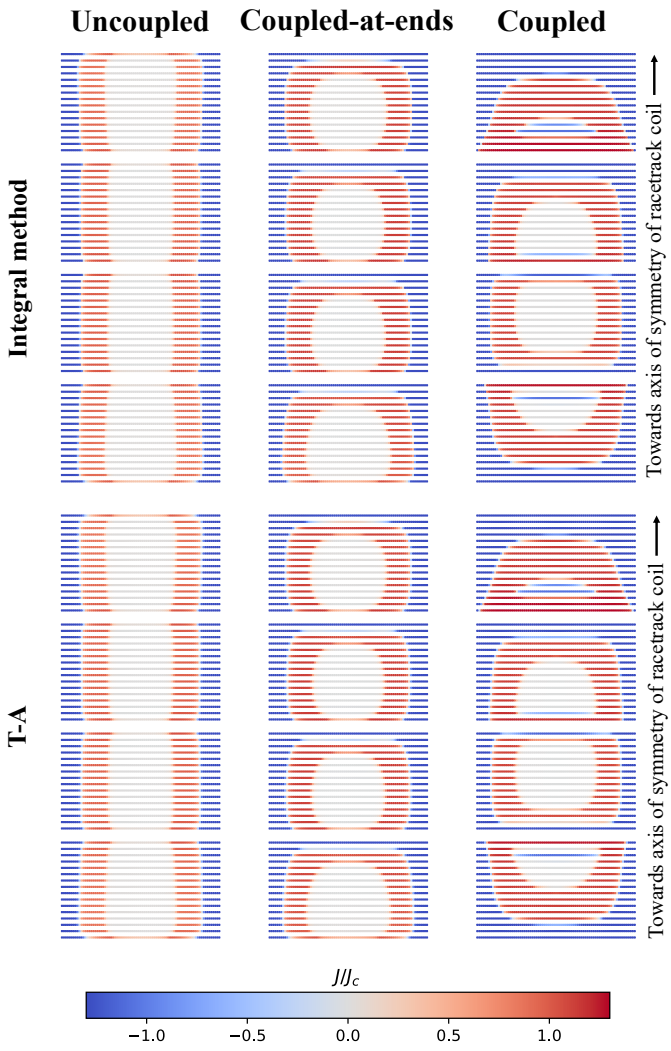

Fig. 3: Current (J/J_c) distribution of the three coupling scenarios at $t = 0.001$ s calculated by the integral method and T-A formulation.

to model terminal resistance in our equivalent circuit or by modifying the E field definition in the integral method may be possible extensions to this paper.

In Fig. 2 for the coupled case, we have assumed zero contact resistance between the tapes, as tapes are connected with the dotted lines (which represent wires) without resistors. Thus, we assume that current is able to switch between tapes without resistance at one of the two end-turns, which are not modelled in our 2D model of the racetrack coil; but each tape keeps the same transport current in the two straight sections of a cable turn, since the 2D model assumes the straight sections of the racetrack coil extend infinitely into the page. In the future, contact resistance can be modelled using a partial element equivalent circuit (PEEC) as used when modelling non-insulated (NI) coil [12], [19] and parallel-wound NI coil [20]. The PEEC approach divides the coil into small elements; resistors connect elements of neighboring tapes to model contact resistance.

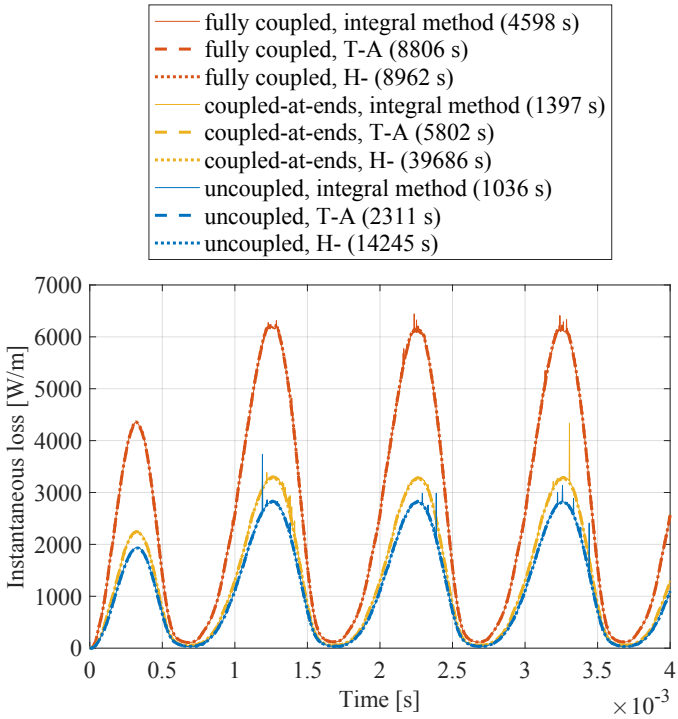

Fig. 4: Instantaneous ac loss of one side of a racetrack coil carrying transport ac, for different coupling scenarios of the coil and calculated via different methods. The time taken by each method is shown in brackets in the legend. Computer specifications: Intel i7-8700 CPU @ 3.2 GHz 3.19 GHz; 32 GB RAM; Windows 10 Enterprise; COMSOL 6.0; Python 3.11, Spyder 5.4.2.

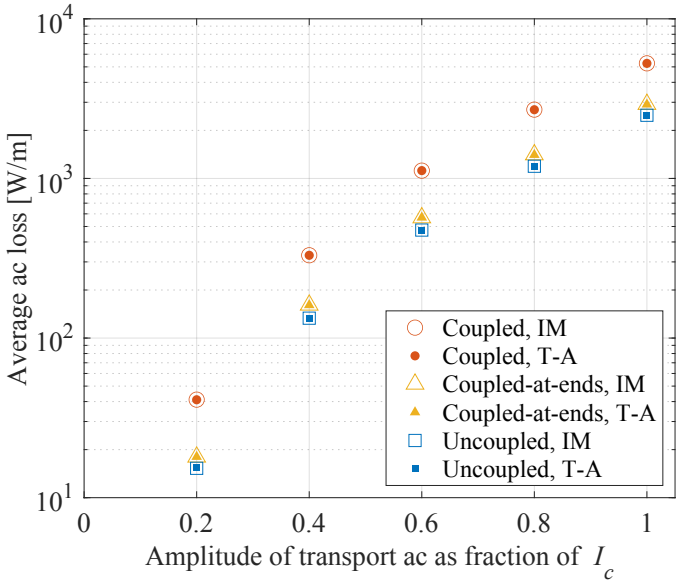

Fig. 5: Average ac loss of one side of a racetrack coil carrying transport ac in the second half of the first period simulated. "IM" stands for integral method.

B. Applicability to other numerical methods

The equivalent circuit used in Santos *et al.* [9] and in this paper may potentially be coupled with numerical methods

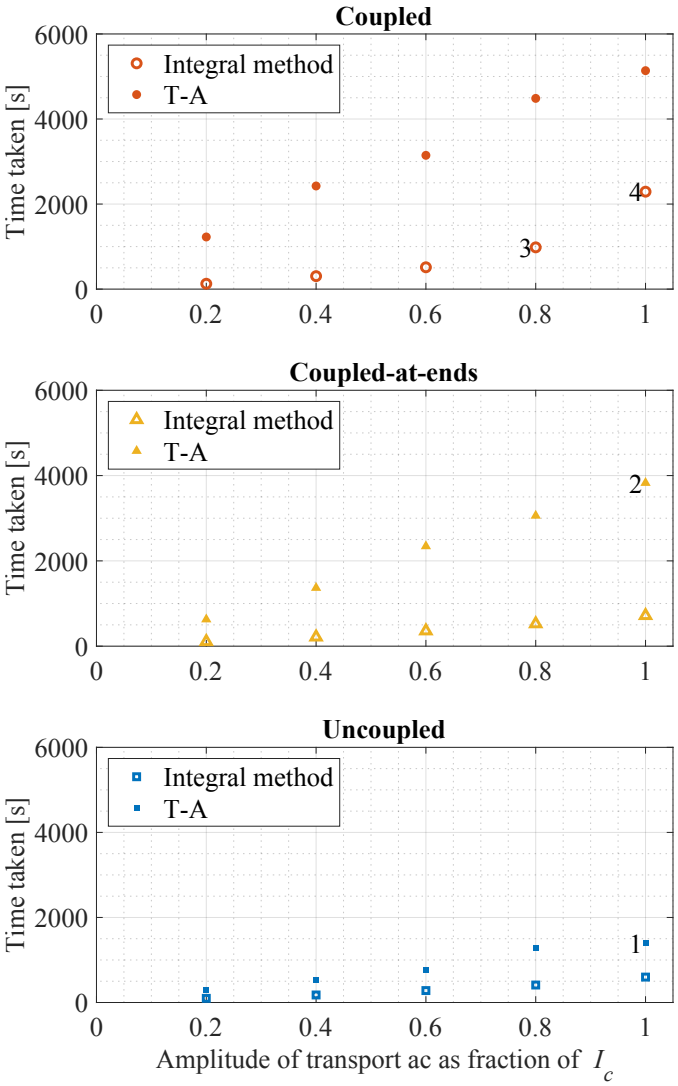

Fig. 6: Time taken by the integral method and T-A formulation to calculate ac loss of the racetrack coil. For the T-A formulation calculated via COMSOL, the relative tolerance is set as 1e-4, except for points 1 and 2, for which 1e-5 is used. For the integral method calculated via Python, all data points are calculated by the forward Euler method with (maximum step size, minimum step size) = (1e-6 s, 1e-9 s), except points 3 and 4, which use (1e-7 s, 1e-9 s) and (1e-7 s, 1e-10 s), respectively. Computer specifications are the same as in the caption of Fig. 4.

other than the T-A formulation and integral method. The T-formulation [21] is similar to the integral method in the sense that only the superconductor domain is meshed (i.e., without meshing the air) [22], thus may offer time advantage like the integral method over methods that mesh the air domain. The T-formulation has been implemented using the Galerkin method and backward difference method for discretization in space and time, respectively [23]. The transport current in each tape is imposed by specifying the current potential T at the edges of the tape [23], [24]. In the coupled-at-ends and coupled scenarios, where tapes' current are not known before computation, potentially the tapes' current at each time step can be found by solving a set of equations based on constraints on current and voltage extracted from the equivalent circuit similar to what is presented in Sections III-A and III-B, with voltage taken as $E + \dot{A}$.

VI. Conclusion

In this article, we have extended the integral method to model coils made of HTS tapes that are coupled or coupled-at-ends. In such cases, the current in the tapes are not known prior to solving the model. However, we formulate a set of constraints based on the equivalent circuit proposed by Santos *et al.* [9] for the coupled and coupled-at-ends scenarios, and in this way, we solve for the voltage gradient in the tapes, which are needed in the integral method. The integral method has a time advantage over the existing method of T-A formulation coupled to an equivalent circuit, taking less than 45% of the time of the latter in a wide range of transport ac amplitudes simulated.

Acknowledgment

CCT Chow would like to thank Mr. Muhammad Bin Younas for helpful discussions on use of coupled tapes in machines.

Appendix A
$\underline{\underline{M_{cae}}}$ and $\underline{P_{cae}}$

This appendix explains the details of entries of $\underline{\underline{M_{cae}}}$ and $\underline{P_{cae}}$ in (14). $\underline{\underline{M_{cae}}}$ and $\underline{P_{cae}}$ are filled by considering the three sets of constraints in Section III-A.

A. First set of equations

Substitute (7) in (11),

$$-\sum_{j=1}^{N_t}\left[\left(\frac{\partial\phi(t)}{\partial z}\right)_j \sum_{i=1}^{N_{tic}}\frac{1}{\mu_0}\int_{\Omega_i}\int_{\Omega_j} Q^{-1}(\mathbf{r},\mathbf{r}')\,d^2r'\,d^2r\right] = \dot{I}_{set}(t) - \sum_{i=1}^{N_{tic}}\int_{\Omega_i} s(\mathbf{r},t)\,d^2r. \tag{18}$$

Discretizing (18), we can fill the first row in (14) with

$$\left[\underline{\underline{M_{cae}}}\right]_{1,j} = \sum_{i=1}^{N_{tic}}\left[\underline{\underline{L}}\,\underline{\underline{Q_{inv}}}\,\underline{\underline{L}}^T\right]_{i,j}\Delta x\Delta y \tag{19a}$$

$$\left[\underline{P_{cae}}\right]_1 = \dot{I}_{set} - \sum_{i=1}^{N_{tic}}\left[\underline{\underline{L}}\,\underline{\underline{Q_{inv}}}(\underline{E}+\underline{\dot{A}_a})\right]_i\Delta x\Delta y. \tag{19b}$$

B. Second set of equations

To set $\dot{I}_a = \dot{I}_b$, from (7),

$$\sum_{j=1}^{N_t}\left(\frac{\partial\phi(t)}{\partial z}\right)_j\frac{1}{\mu_0}\left[\int_{\Omega_b}\int_{\Omega_j} Q^{-1}(\mathbf{r},\mathbf{r}')\,d^2r'\,d^2r - \int_{\Omega_a}\int_{\Omega_j} Q^{-1}(\mathbf{r},\mathbf{r}')\,d^2r'\,d^2r\right] = \int_{\Omega_b} s(\mathbf{r},t)\,d^2r - \int_{\Omega_a} s(\mathbf{r},t)\,d^2r. \tag{20}$$

In (12), $\dot{I}_{i+lN_{tic}} = \dot{I}_{i+(l+1)N_{tic}}$, $l = 0, 1, ..., N_{ct} - 2$, and (12) applies to each tape $i = 1, 2, ..., N_{tic}$. These $(N_{ct}-1)N_{tic}$ equations can be implemented by putting $a = [\underline{a}]_k$ and $b = [\underline{a}]_k + N_{tic}$, $k = 1, 2, ..., (N_{ct} - 1)N_{tic}$ in (20) where

$$\begin{aligned}\underline{a} = [&1, && 1 + N_{tic}, && ..., && 1 + (N_{ct} - 2)N_{tic}, \\ &2, && 2 + N_{tic}, && ..., && 2 + (N_{ct} - 2)N_{tic}, \\ &... \\ &N_{tic}, && N_{tic} + N_{tic}, && ..., && N_{tic} + (N_{ct} - 2)N_{tic}]\end{aligned} \tag{21}$$

So far, one row has been filled in (14), and the next $(N_{ct} - 1)N_{tic}$ rows can be filled as follows after discretizing (20):

$$\left[\underline{P_{cae}}\right]_{1+k} = \left(\left[\underline{\underline{L}}\,\underline{\underline{Q_{inv}}}(\underline{E} + \underline{\dot{A}_a})\right]_b - \left[\underline{\underline{L}}\,\underline{\underline{Q_{inv}}}(\underline{E} + \underline{\dot{A}_a})\right]_a\right) \Delta x \Delta y, \tag{22a}$$

$$\left[\underline{\underline{M_{cae}}}\right]_{1+k,j} = \left(\left[\underline{\underline{L}}\,\underline{\underline{Q_{inv}}}\,\underline{\underline{L}}^T\right]_{a,j} - \left[\underline{\underline{L}}\,\underline{\underline{Q_{inv}}}\,\underline{\underline{L}}^T\right]_{b,j}\right)\Delta x \Delta y \tag{22b}$$

$k = 1, 2, ..., (N_{ct} - 1)N_{tic}, a = [\underline{a}]_k, b = [\underline{a}]_k + N_{tic}$.

C. Third set of constraints

Equation (13) can be rewritten as

$$\sum_{j=0}^{N_{ct}-1} \left(\frac{\partial \phi}{\partial z}\right)_{k+jN_{tic}} - \sum_{j=0}^{N_{ct}-1} \left(\frac{\partial \phi}{\partial z}\right)_{k+1+jN_{tic}} = 0, \quad k = 1, 2, ..., N_{tic} - 1. \tag{23}$$

So far, $1 + (N_{ct} - 1)N_{tic}$ rows have been filled in (14), and the remaining $N_{tic} - 1$ rows can be filled by considering (23) as follows.

$$\left[\underline{\underline{M_{cae}}}\right]_{1+(N_{ct}-1)N_{tic}+k,l} = \begin{cases} 1, & l = k + jN_{tic}, \quad \forall j = 0, 1, ..., N_{ct} - 1 \\ -1, & l = k + 1 + jN_{tic}, \ \forall j = 0, 1, ..., N_{ct} - 1 \\ 0, & \text{otherwise} \end{cases}, \tag{24a}$$

$$\left[\underline{P_{cae}}\right]_{1+(N_{ct}-1)N_{tic}+k} = 0, \quad k = 1, 2, ..., N_{tic} - 1. \tag{24b}$$

APPENDIX B
$\underline{\underline{M_c}}$ AND $\underline{P_c}$

This appendix explains the details of entries of $\underline{\underline{M_c}}$ and $\underline{P_c}$ in (17). $\underline{\underline{M_c}}$ and $\underline{P_c}$ are filled by considering the two sets of constraints in Section III-B.

A. First set of constraints

The first set of constraints, i.e., (15) for $i = 1, 2, ..., N_{ct}$, can be rewritten

$$\left(\frac{\partial \phi}{\partial z}\right)_d - \left(\frac{\partial \phi}{\partial z}\right)_{d+1} = 0, \quad d = [\underline{d}]_k, k = 1, 2, ..., (N_{tic} - 1)N_{ct}, \tag{25}$$

where

$$\begin{aligned}\underline{d} = [&1, && 2, && ..., && N_{tic} - 1, \\ &N_{tic} + 1, && N_{tic} + 2, && ..., && N_{tic} + N_{tic} - 1, \\ &2N_{tic} + 1, && 2N_{tic} + 2, && ..., && 2N_{tic} + N_{tic} - 1, \\ &... \\ &(N_{ct} - 1)N_{tic} + 1, ..., && (N_{ct} - 1)N_{tic} + N_{tic} - 1]\end{aligned} \tag{26}$$

Therefore, (25) can be implemented as

$$\left[\underline{\underline{M_c}}\right]_{k,l} = \begin{cases} 1, & l = [\underline{d}]_k \\ -1, & l = [\underline{d}]_k + 1 \\ 0, & \text{otherwise} \end{cases} \tag{27a}$$

$$\left[\underline{P_c}\right]_k = 0 \tag{27b}$$

$k = 1, 2, ..., (N_{tic} - 1)N_{ct}$.

B. Second set of constraints

Let vector $\underline{g}$ be a function of k, $\underline{g}(k) = [(k-1)N_{tic} + 1, (k-1)N_{tic} + 2, (k-1)N_{tic} + 3, ..., (k-1)N_{tic} + N_{tic}]$. Then, (16) is $\sum_{\forall g \in \underline{g}} \dot{I}_g = \dot{I}_{set}$, which can be rewritten as

$$-\sum_{j=1}^{N_t} \left[\left(\frac{\partial \phi(t)}{\partial z}\right)_j \sum_{\forall g \in \underline{g}} \frac{1}{\mu_0} \int_{\Omega_g} \int_{\Omega_j} Q^{-1}(\mathbf{r}, \mathbf{r}')\, d^2r'\, d^2r\right] = \dot{I}_{set}(t) - \sum_{\forall g \in \underline{g}} \int_{\Omega_g} s(\mathbf{r}, t)\, d^2r. \tag{28}$$

So far, $(N_{tic} - 1)N_{ct}$ rows have been filled in (17), and the remaining rows can be filled with the N_{ct} equations of (16), considering the form (28) above:

$$\left[\underline{\underline{M_c}}\right]_{(N_{tic}-1)N_{ct}+k,j} = \sum_{\forall g \in \underline{g}(k)} \left[\underline{\underline{L}}\,\underline{\underline{Q_{inv}}}\,\underline{\underline{L}}^T\right]_{g,j} \Delta x \Delta y \tag{29a}$$

$$\left[\underline{P_c}\right]_{(N_{tic}-1)N_{ct}+k} = \dot{I}_{set} - \sum_{\forall g \in \underline{g}(k)} \left[\underline{\underline{L}}\,\underline{\underline{Q_{inv}}}(\underline{E} + \underline{\dot{A}_a})\right]_g \Delta x \Delta y \tag{29b}$$

$k = 1, 2, ..., N_{ct}$

REFERENCES

[1] H. Miyazaki *et al.*, "Fabrication and test of a 400 kW-class fully superconducting synchronous motor using REBCO tape for an electric propulsion system," *IEEE Trans. Appl. Supercond.*, 2024, Art. no. 5200506.

[2] S. Miura *et al.*, "Development and assessment of simplified analytical method for current distribution among $REBa_2Cu_3O_y$ parallel conductors in armature windings for fully superconducting rotating machines," *Supercond. Sci. Technol.*, vol. 36, no. 6, 2023, Art. no. 065007.

[3] T. Qu *et al.*, "Development and testing of a 2.5 kW synchronous generator with a high temperature superconducting stator and permanent magnet rotor," *Supercond. Sci. Technol.*, vol. 27, no. 4, 2014, Art. no. 044026.

[4] Y. Statra, H. Menana, B. Douine, and T. Lubin, "Axial-field synchronous machine with HTS armature windings: realization and preliminary tests," *IEEE Trans. Appl. Supercond.*, vol. 32, no. 4, 2022, Art. no. 5200405.

[5] F. Grilli *et al.*, "Superconducting motors for aircraft propulsion: the advanced superconducting motor experimental demonstrator project," *Journal of Physics: Conference Series*, vol. 1590, 2020, Art. no. 012051.

[6] F. Weng, M. Zhang, T. Lan, Y. Wang, and W. Yuan, "Fully superconducting machine for electric aircraft propulsion: study of ac loss for HTS stator," *Supercond. Sci. Technol.*, vol. 33, no. 10, 2020, Art. no. 104002.

[7] C. C. T. Chow, M. D. Ainslie, and K. T. Chau, "High temperature superconducting rotating electrical machines: An overview," *Energy Rep.*, vol. 9, pp. 1124–1156, 2023.
[8] E. Pardo, F. Grilli, Y. Liu, S. Wolftadler, and T. Reis, "AC loss modeling in superconducting coils and motors with parallel tapes as conductor," *IEEE Trans. Appl. Supercond.*, vol. 29, no. 5, 2019, Art. no. 5202505.
[9] B. M. O. Santos *et al.*, "2-D modeling of HTS coils with T-A formulation: How to handle different coupling scenarios," *IEEE Trans. Appl. Supercond.*, vol. 32, no. 5, 2022, Art. no. 5900804.
[10] A. Kobun *et al.*, "Basic concept for uniform current distribution in parallel conductors by introducing a small number of transpositions in REBCO armature coils," *IEEE Trans. Appl. Supercond.*, vol. 33, no. 5, 2023, Art. no. 5200406.
[11] S. Hahn, D. K. Park, J. Bascunan, and Y. Iwasa, "HTS pancake coils without turn-to-turn insulation," *IEEE Trans. Appl. Supercond.*, vol. 21, no. 3, pp. 1592 – 1595, 2011.
[12] Y. Wang, W. K. Chan, and J. Schwartz, "Self-protection mechanisms in no-insulation (RE)$Ba_2Cu_3O_x$high temperature superconductor pancake coils," *Supercond. Sci. Technol.*, vol. 29, no. 4, 2016, Art. no. 045007.
[13] V. Zermeno, P. Krüger, M. Takayasu, and F. Grilli, "Modeling and simulation of termination resistances in superconducting cables," *Supercond. Sci. Technol.*, vol. 27, no. 12, 2014, Art. no. 124013 .
[14] S. Wang, H. Yong, and Y. Zhou, "Calculations of the AC losses in superconducting cables and coils: Neumann boundary conditions of the T–A formulation," *Supercond. Sci. Technol.*, vol. 35, no. 6, 2022, Art. no. 065013.
[15] E. H. Brandt, "Superconductors of finite thickness in a perpendicular magnetic field: Strips and slabs," *Phys. Rev. B*, vol. 54, no. 6, pp. 4246–4264, 1996.
[16] L. Lai and C. Gu, "AC loss calculation in REBCO coils or stacks by solving the equation of motion for current using an integration approach," *Supercond. Sci. Technol.*, vol. 34, no. 1, 2021, Art. no. 015003.
[17] C. C. T. Chow, F. Grilli, and K. T. Chau, "Numerical modelling of HTS tapes under arbitrary external field and transport current via integral method: review and application to electrical machines," *Supercond. Sci. Technol.*, vol. 36, no. 11, 2023, Art. no. 115027.
[18] S. Otten and F. Grilli, "Simple and fast method for computing induced currents in superconductors using freely available solvers for ordinary differential equations," *IEEE Trans. Appl. Supercond.*, vol. 29, no. 8, 2019, Art. no. 8202008.
[19] T. Wang *et al.*, "Analyses of transient behaviors of no-insulation rebco pancake coils during sudden discharging and overcurrent," *IEEE Trans. Appl. Supercond.*, vol. 25, no. 3, 2015, Art. no. 4603409.
[20] Y. Fu, Y. Wang, W. Peng, Y. Zhao, G. Ma, and Z. Jin, "Non-uniform current distribution in parallel-wound no-insulation high-temperature superconductor coil during ramping and fast discharging operations," *Supercond. Sci. Technol.*, vol. 36, no. 11, 2023, Art. no. 115031.
[21] Y. Ichiki and H. Ohsaki, "Numerical analysis of ac losses in YBCO coated conductor in external magnetic field," *Phys. C: Supercond.*, vol. 412-414, pp. 1015–1020, 2004.
[22] H. Ueda, M. Fukuda, K. Hatanaka, W. Tao, A. Ishiyama, and S. Noguchi, "Spatial and temporal behavior of magnetic field distribution due to shielding current in HTS coil for cyclotron application," *IEEE Trans. Appl. Supercond.*, vol. 23, no. 3, 2013, Art. no. 4100805.
[23] K. Kajikawa *et al.*, "Feasibility study on a new three-phase power transmission cable with radial arrangement of superconducting tapes," *Physica C: Superconductivity and its Applications*, vol. 445-448, pp. 1058–1061, 2006.
[24] N. Amemiya and K. Akachi, "Magnetic field generated by shielding current in high t_c superconducting coils for NMR magnets," *Supercond. Sci. Technol.*, vol. 21, no. 9, 2008, Art. no. 095001.